Hydrothermal Synthesis and Magnetic Properties of Copper-doped Lead Apatite

Wang Hongyang[1, *], Wu Hao[2], Wu Zhixing[3], Geng Zhihui[4], Zhou Juncheng[1], Deng Ziqi[5], Yan Liqin[6], Qian Peng[1], Ye Shufeng[1], Shi Ke[7], Chen Ning[8, *]

1. State Key Laboratory of Multiphase Complex Systems, Institute of Process Engineering, Chinese Academy of Sciences, Beijing, China.
2. State Key Laboratory of Material Processing and Die & Mold Technology, School of Materials Science and Engineering, Huazhong University of Science and Technology (HUST), Wuhan, China.
3. Fujian Provincial Key Laboratory of Analysis and Detection Technology for Food safety, College of Chemistry, Fuzhou University, Fuzhou, China.
4. School of Engineering, Course of Applied Science, Tokai University, Hiratsuka, Japan.
5. School of Materials Science and Engineering, Northeastern University, Shenyang, China.
6. Beijing National Laboratory for Condensed Matter Physics, Institute of Physics, Chinese Academy of Sciences, Beijing, China.
7. Beijing 2060 Technology Co., Ltd, Beijing, China
8. School of Materials Science and Engineering, University of Science and Technology Beijing, Beijing, China

*Corresponding Author: Cheng N and Wang H.

E-mail: wanghy@ipe.ac.cn

Tel. and Wechat: +86-17710349134

Abstract

This study synthesized copper-substituted lead apatite using the hydrothermal method, starting from hydroxyapatite precursors. For stability, it is recommended to maintain copper substitution below x=2 in the $Pb_{10-x}Cu_x(PO_4)O$ apatite. The introduction of copper appropriately reduces the lattice constant, in line with DFT theoretical calculations. Non-equilibrium heat treatment introduces additional charge carriers; oxygen-rich tempering shifts the sample to paramagnetism, while anaerobic tempering leads to complex and unique hysteresis loops. Non-equilibrium annealing can increase carrier concentration, but its efficacy is limited. Although some improvements have

been observed, further exploration involving additional element doping or seeking interfaces with suitable conductive phases is needed to achieve superconductivity.

1. Introduction

The so-called LK99 system is not purely composed of lead apatite; different amounts of copper can replace lead, and there are also nano-phases such as Cu_2S, Pb, and Cu[1]. To analyze the origin of its peculiar properties, it is necessary to first study the single-phase problem. Currently, the MPI's single crystal [2] is considered a pure single phase, while other studies involve multiple phases[3, 4].

These studies primarily measure electrical and magnetic properties, suggesting that the main phase is a semiconductor[5]. However, even with the same copper substitution, V.P.S. Awana 's team using Hall effect measurements [6] identified a hole-type gap of 0.52 eV and a very small carrier concentration of 10^(-14), whereas PKU's temperature-dependent resistivity curve for copper substitution showed a gap around 0.2 eV, indicating a narrow-band semiconductor[7].

On the other hand, quantum mechanical calculations are based on lead apatite as the mother matrix [8, 9], with most conclusions confirming a flat band in the Fermi level, favoring superconductivity. However, in pure phases with a bandgap above 2 eV, copper substitution is relied upon to reduce the bandgap. Additionally, the substitution of copper at different lead positions introduces variations, allowing for the manipulation of Fermi surface carrier concentration using atomic control.

In summary, both experimental and theoretical studies indicate that copper substitution in lead apatite significantly influences the comprehensive performance of the system. However, the specific impact of the quantity of copper substitution on the magnetic properties of the system is still unclear.

Therefore, it is necessary to synthesize single-phase materials with different copper substitution levels to understand the regular variations in their performance. **Furthermore, non-equilibrium methods[10]** can be employed to increase the carrier concentration in the apatite system, facilitating a more in-depth analysis of the unique properties of LK99 (Copper-doped lead apatite) .

2. Experimental

2.1 Synthesis

(1) Stable Sample Preparation Method

Solution A: Prepare a mixed solution of 100 ml containing $Pb(NO_3)_2$ and $Cu(NO_3)_2$, with a concentration of 0.15 mol/L for (Pb^{2+} + Cu^{2+}).Solution B: Prepare a 100 ml solution of 0.1 mol/L Na_2HPO_4, and adjust the pH to 11 using NaOH. Solution C: Prepare a 100 ml solution of 0.15 mol/L Na_2EDTA, and adjust the pH to 8 to ensure complete dissolution of EDTA.

Step 1: Mix solution A with solution C, and adjust the pH to 10. Stir the solution for at least 3 hours at 60°C in a water bath to allow thorough chelation of copper and lead ions with EDTA. Step 2: Add solution B to the mixture of solutions A and C. Stir the mixture at 60°C for 12 hours. After the first hydrothermal step, check the color of the hydrothermal sample. As the Pb/Cu ratio decreases, the turbidity deepens, appearing grayish-brown. If the sample is too brown, the Pb-Cu chelation has failed, and the solution needs to be reconfigured. Step 3: Place the mixture prepared in Step 2 in a high-pressure hydrothermal reactor. Hydrothermally treat at 160°C to 180°C for 24 hours, with a hydrothermal pressure greater than 3 MPa, ranging from 3 to 6 MPa. Allow natural cooling after hydrothermal treatment. After hydrothermal treatment, check the turbidity color again. If there is no lightening of weak color, re-hydrothermal treatment or solution reconfiguration is needed. Step 4: Wash, filter, and dry the powdered sample. The obtained powdered sample at this point is hydroxyapatite containing lead and phosphorus, with the chemical formula $Pb_{10-x}Cu_x(PO_4)_6(OH)_2$.Step 5: Place the powdered sample in a quartz crucible for the first-stage calcination. The temperature for the first-stage calcination is 900°C, and the sample is kept at this temperature for 12 hours to complete the dihydroxylation reaction. Step 6: After grinding and crushing the sample prepared in Step 5, press it into a block and calcine at 850°C for 12 hours to achieve caramelization and densification.

(2) Non-Equilibrium Sample Preparation Method

The non-equilibrium preparation of $Pb_{10-x}Cu_x(PO_4)6O_{(1+y)}$, y=0~1, is carried out using a bubble oxygen process. Steps 1 to 4 are the same as described above. Step 5: Place

the powdered sample in a quartz crucible for the first-stage calcination. The temperature for the first-stage calcination is 900°C. After reaching 900°C, switch the atmosphere to pure oxygen and maintain the temperature for 12 hours. Step 6: After grinding and crushing the sample prepared in Step 5, press it into a block. Perform pure oxygen calcination at 500°C for 48 hours. After the oxygen bubbling process, use liquid nitrogen for rapid cooling.

The experimental sample numbers and specific synthesis conditions are provided in Table 1 and Table 2 at the end of the article.

2.3 Characterization and DFT

The XRD patterns were recorded through a Rigaku Ultima IV diffractometer with a Cu-Kα radiation (λ=1.54059 Å, 40 kV, 40.0 mA) for the solid samples. Data were collected in 2θ range 5-90° at a scan rate of 0.02°/step. Processing of data was conducted using Reflex.

Transmission electron microscopy (TEM) were used to determine the morphology of Apatite using an acceleration voltage of 200 kV. Energy-dispersive X-ray spectroscopy (EDX) was performed with an EDS detector on TEM.

The magnetic properties of the samples were investigated using the VSM module in the PPMS and the SQUID module in the MPMS. M-T curves were obtained with a temperature change rate of 1 K/min, providing insights into the variations in magnetization with temperature. For M-H curve measurements, the VSM module in PPMS was employed in the magnetic field waiting mode, replacing the sweep mode to enhance precision. This mode allowed for a more accurate analysis of magnetic properties under varying magnetic fields.

The EPR spectra were recorded at room temperature on a conventional X-band Bruker ELEXSYS E 500 CW-spectrometer operating at 9.46 GHz with a 100 kHz magnetic field modulation.

CASTEP is employed for optimizing crystal structures by minimizing the total energy of the system with respect to atomic positions and unit cell parameters. The electronic exchange-correlation interactions are treated using the Generalized Gradient Approximation (GGA), specifically parameterized by the Perdew-Burke-Ernzerhof

(PBE) method. Through an iterative process, the calculations converge to the minimum total energy, resulting in the optimal crystal structure.

3. Discussion

3.1 Copper-Doped apatite Crystal Structure Analysis

Figure 1 shows the XRD pattern of the sample, with crystal structure refining by Reflex. As the substitution ratio of Cu in lead apatite increases, there is a decreasing trend in the lattice parameters of the sample. The crystal structure of copper-doped apatite was optimized by CASTEP, and the theoretical trends match the experimental values **(Figure (h) and (i))**. The experimental lattice parameters of lead apatite reported by LK99 are a=9.843 and c=7.428, showing differences from the current experimental sample. It is noteworthy that when the Cu/Pb ratio exceeds 0.25, the decrease in the experimental sample's lattice parameters is not linear; the magnitude of the change diminishes. Copper incorporation has gradually reached saturation, consistent with reported data in $Pb_{10-x}Cu_x(PO_4)_6O$ where x should be less than 2.

After non-equilibrium soaking, the lattice parameters of the sample are shown in **Figure 1(k)**. Adding or removing additional oxygen atoms to the system and optimizing its structure using CASTEP result in calculated lattice parameters as shown in **Figure 1(j)**. When there is an excess of oxygen in the system, prolonged exposure to oxygen leads to slight contraction of the crystal and a corresponding reduction in lattice parameters. After annealing in argon, the sample undergoes some degree of deoxygenation, causing the crystal to expand, and lattice parameters increase. The experimental results align with theoretical predictions. Theoretical calculations suggest that under oxidative conditions, Cu is more likely to replace Pb (M2) sites, while soaking in argon or annealing in air makes Cu more likely to replace Pb (M1) sites **(Figure 1 (i), (m), and (n))**. Theoretical calculations are only used for qualitative analysis and are not the main focus of this paper.

Pure lead apatite prepared by element doping or non-equilibrium methods may not achieve the lattice paraments reported by LK99. This implies the possible presence of a second element (S, F, Cl, etc.) in the crystal lattice, or partial substitution of phosphate groups by sulfate in the system. This can explain why Li's method[1] mentions the use

of Pb_2SO_5 and Cu_3P.

Although the same synthesis method was employed, subtle differences in lattice paraments and crystallinity persist between Sample 1 and Sample 2. These slight distinctions may ultimately result in noticeable variations in their magnetic properties.

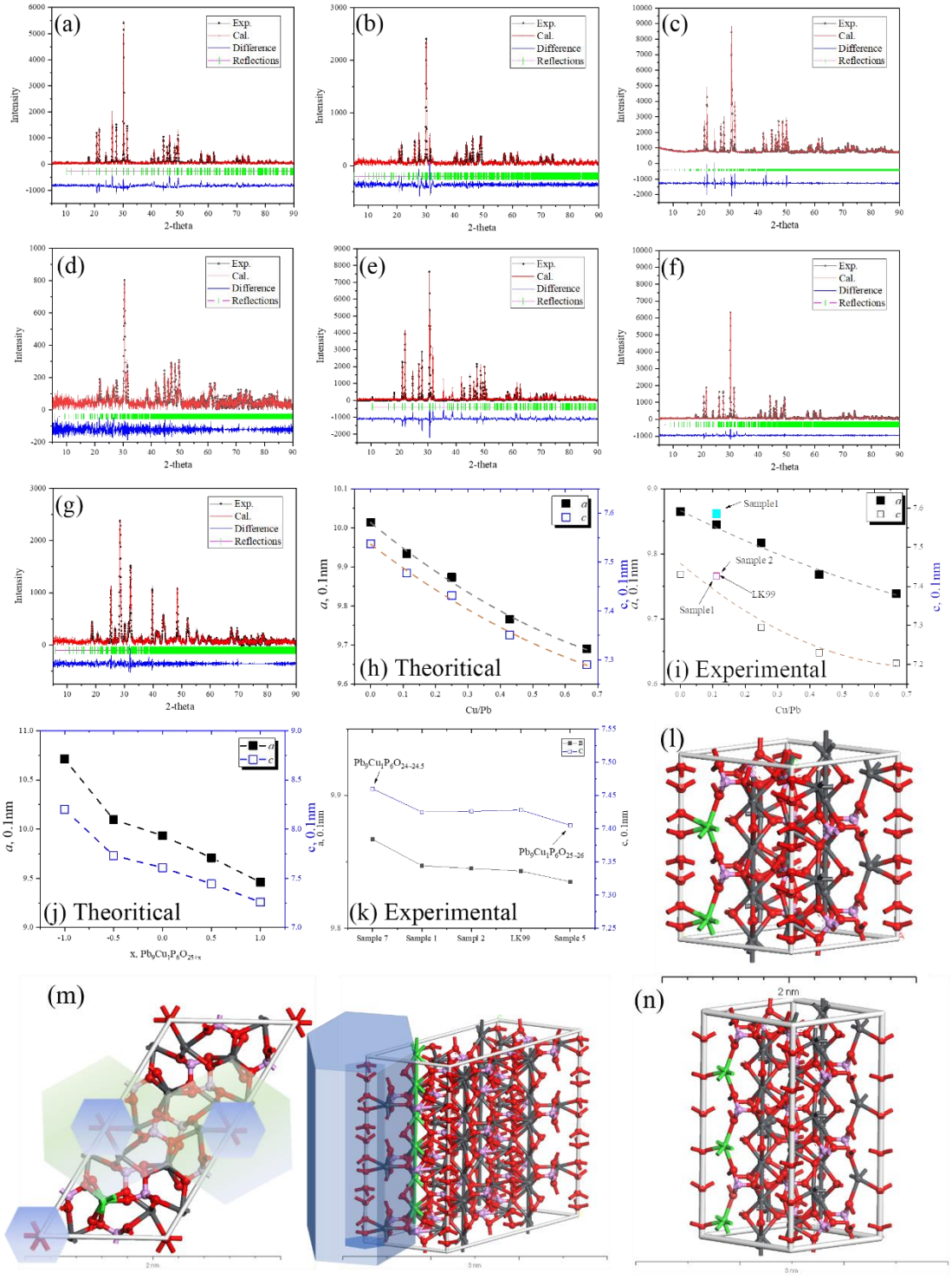

Figure 1: Experimental sample XRD patterns and lattice parameters. (a)-(g) correspond to the XRD patterns of samples 1 to 7, (g) CASTEP-calculated lattice

parameters of $Pb_{10-x}Cu_xP_6O_{25}$, (i) experimental lattice parameters of $Pb_{10-x}Cu_xP_6O_{25}$, (j) CASTEP-calculated non-equilibrium sample lattice constants, (k) comparison of lattice parameters for $Pb_9Cu_1P_6O_{25\pm x}$, (l) schematic representation of the optimized structure of $Pb_9Cu_1P_6O_{25}$, (m) $Pb_9Cu_1P_6O_{26}$, and (n) $Pb_9Cu_1P_6O_{24.5}$.

Transmission electron microscopy tests were conducted on samples 6 and 7, showing in **Figure 2**. Electron diffraction indicates that the sample exhibits single-crystal characteristics in microscopic regions, but at an enlarged scale, the crystal orientation becomes complex. Even though there is a one-dimensional conducting path in the sample, direct measurements using four-electrode or two-electrode methods were not achievable. As shown in **Figure 2(d)**, the spacing between crystal planes is unstable, and this condition may be related to the random substitution of copper or the uneven doping of copper at the atomic scale. From the results of EDS (**Figure (g) and (h)**), the hydrothermal method excluded the possibility of Pb and Cu exclusion during the previous sample preparation, confirming that Cu fully replaces Pb in the apatite structure. However, whether the substitution of Cu is uniform and the positions are rational still requires further in-depth characterization analysis.

It's worth noting that due to the instability of phosphates, using a series of electron beam devices such as AC-TEM for characterization may lead to the sample's decomposition. Visualizing and characterizing the substitution sites and uniformity of Cu might still be a challenging task.

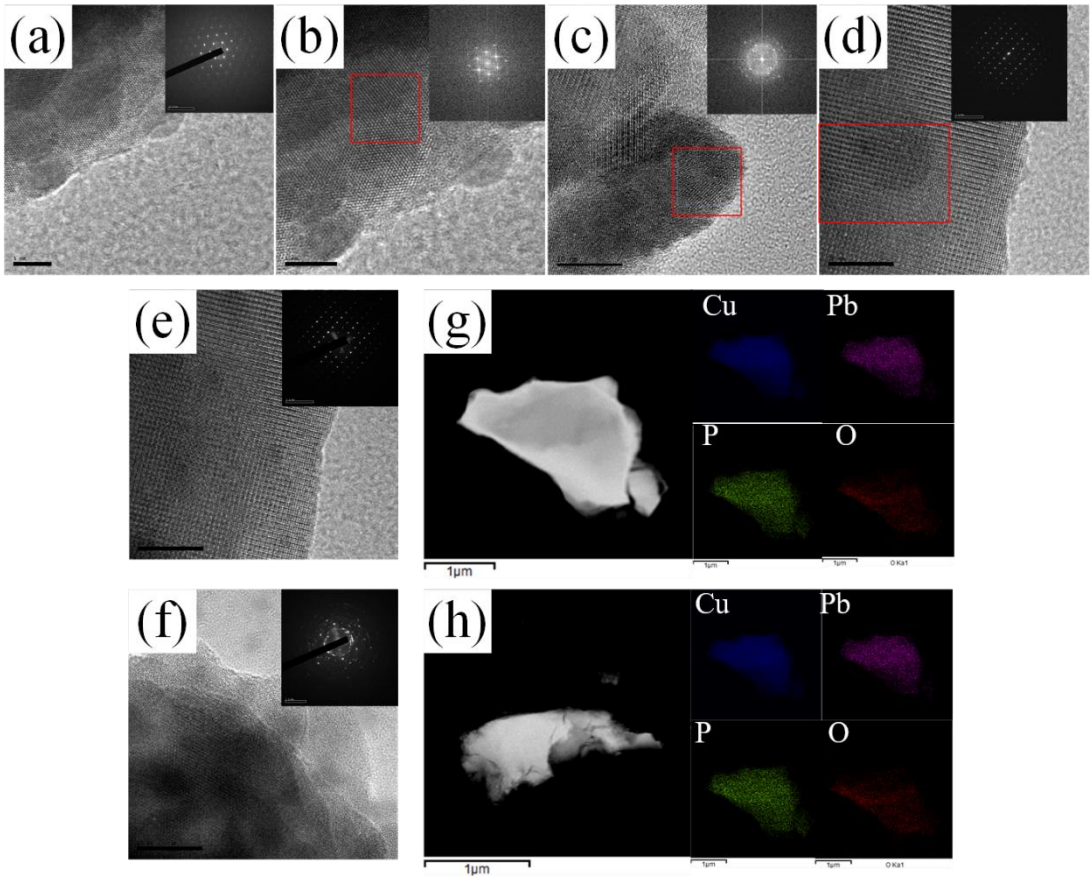

Figure 2. Transmission Electron Microscopy (TEM) spectra showing (a) to (c) TEM samples of Sample 6, (d) to (f) TEM samples of Sample 7, and (g) and (h) Energy-Dispersive X-ray Spectroscopy Mapping of Sample 7.

3.2 Copper-Doped Apatite Magnetic Properties

(1) Magnetic Properties of Stable Samples

We measured the M-T of samples 1, 2, and 4 and obtained the magnetic hysteresis loops (M-H) at 300K (**Figure 3**). No significant magnetic transitions were observed in the M-T tests of samples 1 and 4. They exhibited paramagnetism or weakly diamagnetism behavior at room temperature, and paramagnetism behavior at low temperatures.

The inability to achieve the magnetic properties reported in LK99 may be related to deviations in crystal structure. The M-H curves of the samples showed a combination of diamagnetism and extremely weak ferromagnetic behavior, possibly related to the nonzero spin magnetic moment of Cu[11]. Copper doping in samples prepared by hydrothermal synthesis occurs randomly and cannot fully control the orientation of the M1 or M2 sites in lead apatite. This weak magnetism may also be caused by the

precipitation of nano CuO particles[11].

Samples 2 and 1 were synthesized using the same method, but they exhibited significant differences in magnetic properties. At 300K, sample 2 showed metallic-like diamagnetism. Despite the lack of conductivity in the sample, this diamagnetic behavior may be caused by the presence of internal free electron pathways. During the sample testing, it was observed that their magnetic hysteresis loops could not overlap (field waiting mode). This result was mainly caused by PPMS testing errors. The lattice parameters of sample 2 are close to those of LK99, and a suitable crystal structure (more appropriate doping positions) may be the reason for the enhancement of diamagnetism.

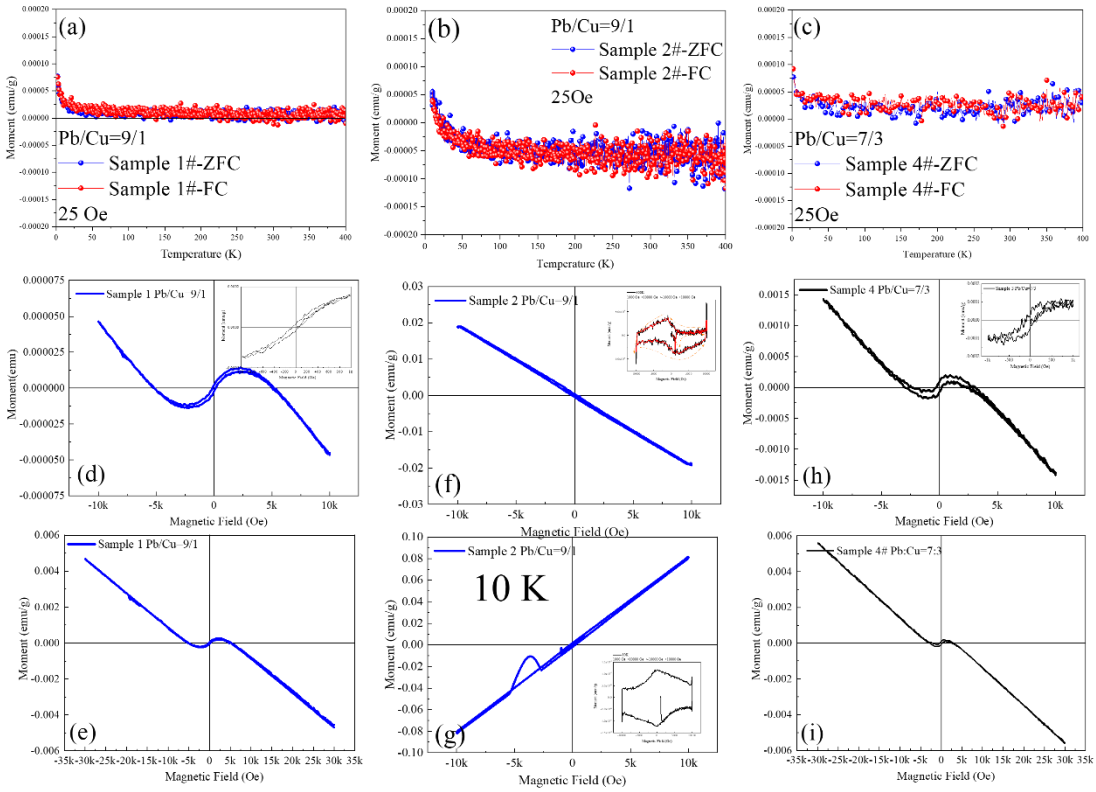

Figure 3 M-T and M-H curve (a) Sample 1 M-T (b) Sample 2 M-T (c) Sample 4 M-T (d) Sample 1 M-H, 300K,1T (e) Sample 1 M-H, 300K, 3T (f) Sample 2 M-H, 300K,1T (g) Sample 2 M-H, 10K, 1T(h) Sample 4 M-H, 300K,1T (i) Sample 4 M-H, 300K, 3T.

The magnetic properties of the apatite samples synthesized by hydrothermal method are basically similar to those reported in previous literature

(2) Magnetic Properties of Non-equilibrium Samples

In contrast to stable samples, after prolonged exposure to an oxygen atmosphere and oxygen soaking, sample 6 undergoes a transition from diamagnetic to paramagnetic behavior. Excess oxygen atoms provide free electrons to the system, leading to the formation of a paramagnetic state. Despite oxygen soaking, ferromagnetic characteristics still persist in the sample, and the magnetic hysteresis loops do not completely overlap within 2000 Oe. This pattern can be explained as the superposition of paramagnetism and ferromagnetism, or as layered magnetism related to semiconductors[11] or spin glass[12]. Although in actual measurements, the initial magnetization curve shifts towards negative values when the magnetic field is within 500Oe, this cannot be explained as a superconductor as described in the literature[13].

The ZFC-FC curve exhibits a transition step at 300K, which was found to be similar in previous work by the LK method[5].

It is noteworthy that the resistivity of the paramagnetic sample can be measured using the four-probe method, indicating semiconductor behavior. However, the sample becomes ineffective after 14 days in the air. Resistivity data are not reiterated here.

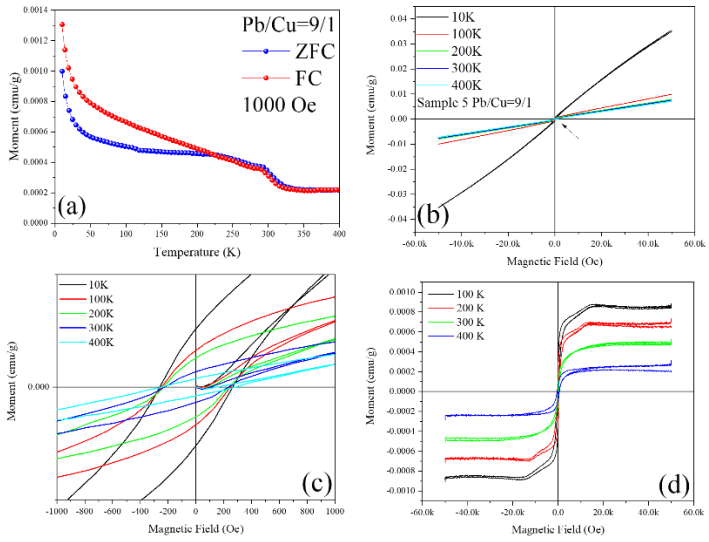

Figure 4 M-T and M-H Curve of Sample 6 (a) M-T (b) M-H, 5T (c) M-H, 0.1T (d) M-H withdraw paramagnetic background

For sample 7, repeated measurements were conducted using both PPMS and SQUID **(Figure 5)**, but the errors introduced during testing could not be completely eliminated. The experiment encountered considerable uncertainty. M-T curves of the sample were

measured using SQUID, no superconducting temperature transition, as observed in the MT curves, was found, and due to equipment limitations, the highest temperature that could be measured was 360 K. The FC curve transforms into paramagnetism, and very few similar curves have been reported in literature[14].

To prevent magnetic damage to the sample, a completely new sample without prior magnetic data was used before magnetic testing. The M-H curve of the first SQUID test is shown in **Figure 5 (b)**, where a magnetic hysteresis loop appeared after 1T. Without changing the sample, a re-measurement is shown in **Figure 5 (c)**. An intriguing phenomenon was observed—in the same test, after one magnetic hysteresis loop, the results of the second test differed significantly from the first test, despite the consistency in the order of magnitude diamagnetism. Similar situations persisted even after changing the equipment. **Figure 5 (f)** shows the opposing ferromagnetic curve observed in the PPMS test, using an entirely new sample unaffected by any magnetic field. After magnetization, the M-H results are shown in **Figures 5 (c) and (d).**

It is challenging to determine whether the test results in **Figure 5 (b) and Figure 5 (e)** were caused **by errors in SQUID and PPMS**, so we avoid overanalyzing the phenomena expressed by these results[15].

It is worth noting that in the opposite magnetic curve of sample 7, the S-shaped pattern is significantly different from samples 1 and 7. Taking sample 1 as an example, we consider it a combination of ferromagnetism and diamagnetism, as previously reported in studies. However, sample 7 exhibits contrary ferromagnetic curve on the basis of the diamagnetic straight line. The M-H curves of the sample were tested at 10K (**Figure 6(d)**), and again, an S-shaped pattern opposite to ferromagnetism was observed. At 10K, the magnetic field strength exhibited diamagnetic behavior within 2.8T. However, this test result appears similar to superconductors with ferromagnetic properties[5, 16].

It is interesting that, as shown in Figure 5 (f), when we subtract a Diamagnetism straight-line background from the curve, we obtain a curve with a similar shape to Figure 5 (d) and Figure 5 (e). Moreover, the numerical values of M-H are essentially similar. Because the sample is not a single crystal, and doping uniformity cannot be guaranteed (as mentioned earlier), it cannot be ruled out whether there is hidden

superconductivity or spin glass in extremely weak signals. As shown in Figure 3 above, copper-doped pyrochlore exhibits paramagnetism at low temperatures and diamagnetism at room temperature. It is worth considering whether special non-equilibrium treatment can effectively increase the carrier concentration, thereby transforming the sample into a ceramic with good conductivity. In Korean literature, the chemical equation for LK99 is given as $Pb_{10-x}Cu_xP_6O_{24}$[17].

For this phenomenon, three possible explanations were considered: (1) weak signals, with actual measurements in the range of 10^(-4) to 10^(-5) emu, causing errors and hysteresis in the test results; (2) the presence of one-dimensional or two-dimensional ferromagnetism, with ferromagnetic regions deviating from the test points causing reverse oscillation; (3) sample magnetization interfering with test results; (4) Short range magnetic ordering caused by crystal defects? (5) the possibility of extremely rare superconducting phases cannot be ruled out, along with the potential coexistence of superconductivity and ferromagnetism.

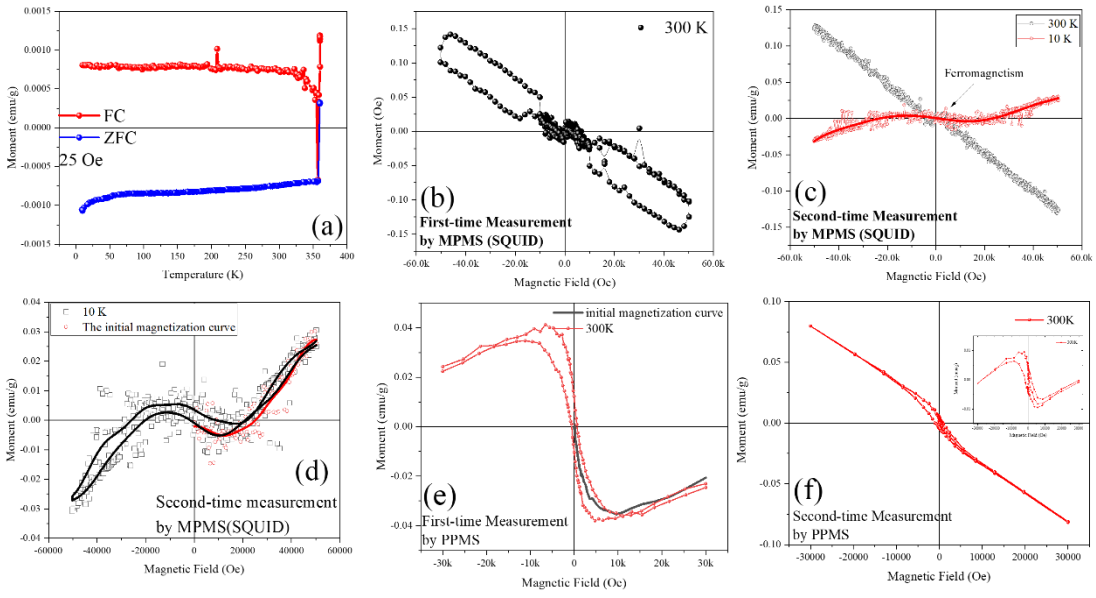

Figure 5 M-T and M-H Curve of sample 7 (a) M-T, 10 to 360K (b) M-H by SQUID at 300K, (c) and (d) M-H by SQUID at 300K and 10 K, (e) M-H by PPMS, 3T, (f) M-H, 3T and withdraw diamagnetic background.

Emphasis: The tested sample's mass was no less than 10mg. Figures 5 (d) and (e) show the measured data without removing any background.

For the convenience of observation, we will provide additional initial magnetization

curves for all M-H tests. As shown in Figure 6. The data after removing the paramagnetic or diamagnetic background from the sample is shown in Figure 6 (b). As shown in Figure 6 (b), we tend to attribute the test results at 300K to strange ferromagnetism.

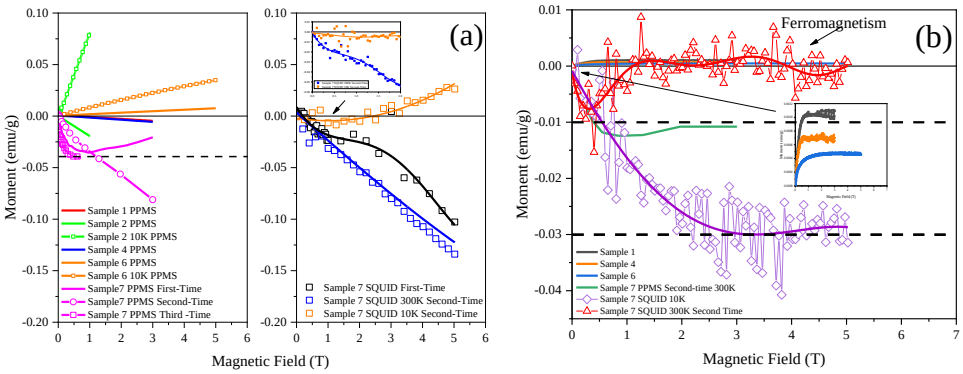

Figure 6 (a) The initial magnetization curve of the samples and (b) after removing paramagnetic or diamagnetic background (Magnetization -0.03emu/g and -0.01 emu/g seems to be a critical point for turning)

3.3 Discussion on EPR Characterization

EPR was employed to confirm the ferromagnetic properties of the samples. Signals around 1700 Oe at room temperature are commonly interpreted as indicative of ferromagnetism, and all samples exhibited distinct ferromagnetic signals. After prolonged oxygen soaking, Sample 6 showed a significant free radical peak at around 3300 Oe [18]. Consequently, the sample transitioned to paramagnetism. Partial copper tetramer structures were observed in the EPR results[19], and the EPR spectra of the samples exhibited significant differences from reported EPR spectra of various superconductors, rejecting the notion of superconductivity. Peaks within 1000 Oe could be explained by the octamer structure of copper or other special structures[20, 21], as shown in Figure 7 (a) and (b). Contrary to Lee's original description of a drastic mutation within 1000 Oe, such a phenomenon did not occur in our experimental samples.

The peak around 200-500, observed in both Sample 6 and Sample 7, is likely associated with ferromagnetism[22]. Literature associates the peaks to itinerant electrons [23] . By integrating the peaks above and below, the ratio suggests the presence of metallic free

electrons. This peak only appears in the sample after non-equilibrium treatment

Presently, EPR test results only support the presence of certain copper structures and ferromagnetic properties. Internal free electrons may exist in Sample 6 or 7, but the test results do not support the existence of a superconducting phase. The EPR data provided by LK99 bear significant resemblance to previously reported DNA data[24], suggesting a possible spiral structure or other characteristics.

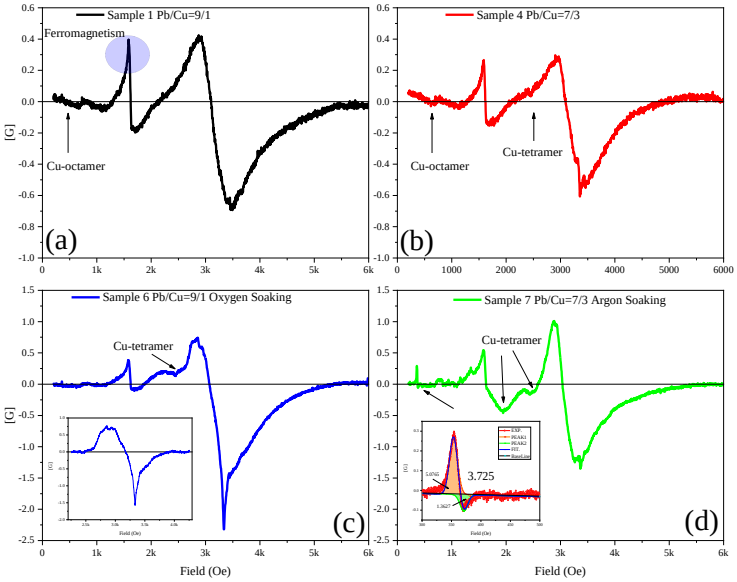

Figure 7 EPR pattern at room temperature (a) Sample 1 (b) Sample 4 (c) Sample 6 (d) Sample 7

3.4 Future and Potential Prospects for Investigation

In our two-month research process, we made diligent efforts to explore the original formula proposed by LK and various experimental methods. We replicated different magnetic behaviors, as shown in Figure 8. However, despite our efforts, conclusive evidence supporting the superconductivity of LK-99 remains elusive, leaving some uncertainty from an experimental perspective.

Apatite was synthesized using the hydrothermal method, followed by calcination in an argon environment and annealing in a vacuum tube. The sample exhibited noticeable lead (Pb) precipitation, as shown in **Figure 8 (c) (resistance jumps were observed in the resistance test near 2~10K)**. Despite this, the sample still exhibited diamagnetism and a distinct magnetic hysteresis loop within 1500 Oe. No detection of cuprous sulfide was found in the sample, but resistance jumps occurred around 280, 300, and 380K.

The possibility of additional conductive phases forming an equivalent circuit with metallic Pb cannot be ruled out. Naturally, this also increases the possibility that impurities or mixed phases may play a significant role in the synthesis of Apatite or their derivatives[25]. Do multiphase combinations, similar to PN junctions or interface superconductors, operate in this material[26]?

Figures 8 (d) to (f) display the magnetic data synthesized using **the method provided by the LK team**. Following the original formula and **Professor Kim Hyun-Tak's advice**, we performed rapid annealing at 1000°C in pure oxygen for 5 minutes. The sample exhibited paramagnetism, but in low magnetic fields (within 200 Oe), the initial magnetization curve of the sample seemed to move towards negative values. This test result does not rule out testing errors in PPMS.

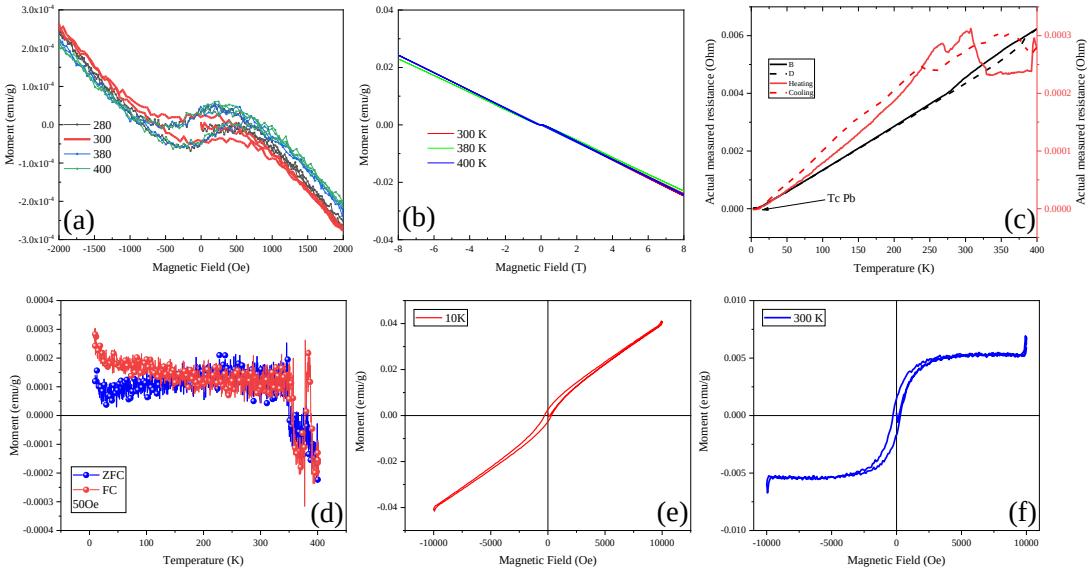

Figure 8 (a) and (b) M-H curves of vacuum-tube-annealed samples, Pb/Cu=9/1, (c) Resistance curve of vacuum-tube-annealed hydroxyapatite sample, Pb/Cu=9/1, (d) MT curve of apatite prepared from $Pb_2(SO_4)O+Cu_3P$, (e) and (f) M-H curves.

Copper-doped apatite exhibits several phenomena, and from an experimental perspective, there are several points worth further exploration:

(1) The stability of the magnetic properties of nearly pure copper-doped lead apatite seems to depend on the copper doping sites. Random doping may introduce ferromagnetism, or spin glass phenomenon.

(2) Direct copper-doped apatite is expected to become an insulator, and introducing

non-equilibrium methods is crucial for providing suitable charge carriers to the system. However, relying solely on oxygen or argon soaking poses challenges in ensuring sample timeliness, with an effective period of approximately 14 days.

(3) Establishing stable charge carriers may play a crucial role in future research. The LK team indicated in the original formula that sulfates and sulfur could be important factors in doping lead apatite.

(4) The synthesis of the original formula exhibits instability, rendering the current global synthesis efforts unable to reproduce. In the context of lead hydroxyapatite, the quantification of copper and sulfur (sulfates) doping remains uncertain. Eliminating interference from impurities and synthesizing single crystals as much as possible should be a scientific experimental approach.

(5) The possibility of coexistence of ferromagnetism and one-dimensional superconducting paths at room temperature cannot be ruled out. The ability to measure the one-dimensional superconducting resistance using the four-probe method poses a challenge for future research[27].

This study primarily investigates the magnetic properties of pure Copper-doped lead apatite and does not negate the potential room temperature superconductivity in LK-99.

4. Conclusion

This article utilized a hydrothermal method to synthesize lead apatite with varying copper substitution ratios, starting from hydroxyapatite precursors. Sintering was employed to obtain the final products, and the XRD results before and after sintering revealed that copper substitution could reach up to 2 atoms, with lattice parameters decreasing as copper content decreased. DFT calculations of lattice constants were consistent with experimental trends for stable and non-equilibrium phases. In the case of sintered apatite systems, characterized by diamagnetic background, some magnetic ordered phases exhibited hysteresis characteristics.

For the oxygen-rich sintered system, XRD indicated a further reduction in lattice parameters, consistent with the lattice trends predicted by DFT theory for composite electronic-type oxygen-doped structures. Magnetic measurements revealed a paramagnetic background. After anaerobic annealing, XRD showed an increase in

lattice parameters, similar to the hole-doped phase predicted by DFT theory. The samples exhibited peculiar magnetic hysteresis loop.

Simultaneously, EPR indicated the presence of free radical electrons in samples subjected to non-equilibrium annealing, suggesting a significant increase in carrier concentration. Pure apatite does not exhibit the metallic conductivity characteristic. Oxygen-rich (anaerobic) sintering significantly improved carrier concentration, revealing a series of distinctive magnetic features, but there still appears to be an insufficient number of carriers (paired electrons) to transition it into a superconductor. If appropriate hole-type (or electron-type) conductive phase interfaces can be utilized, it possibly would contribute to the manifestation of more pronounced superconducting characteristics.

Table

Table 1 $Pb_{10-x}Cu_x(PO_4)_6O$ Synthesis

Sample	Pb/Cu	Bath temperature	Hydrothermal temperature	Roasting Temperature	Atmosphere	Roasting Time
1, 2	9/1	60℃	160℃	900℃	Air	12h
3	8/2					
4	7/3			850℃		
5	6/4					

Table 2. $Pb_{10-x}Cu_x(PO_4)_6O_{(1+y)}$, y=-1~1 Synthesis

Sample	Pb/Cu	Bath Temperature	Hydrothermal Temperature	Atmosphere	Roasting Temperature	Roasting Time	Soaking Temperature	Soaking Time
6	9/1	60℃	160℃	O_2	900℃	12h	500℃	48h
7	9/1	60℃	160℃	Ar	900℃	12h	500℃	48h

Table 3 $Pb_{10-x}Cu_x(PO_4)_6O$ Lattice Parameters

Pb/Cu	Sample	a	c

10/0	Ref	EXP	9.865	7.431
		THE.	10.014	7.537
9/1	**1**	**EXP.**	**9.847**	**7.425**
	2	**EXP.**	**9.845**	**7.426**
		THE.	9.934	7.477
		REF[2].	9.853	7.442
8/2	3	EXP	9.817	7.295
		THE.	9.874	7.431
7/3	4	EXP	9.768	7.230
		THE.	9.766	7.350
6/4	5	EXP	9.739	7.204
		THE.	9.690	7.290
	LK99	**Ref.[1]**	**9.843**	**7.428**

Table 4: Lattice Paraments of Non-equilibrium Samples

Sample	Possibly Phase	Structure		a	c
6	$Pb_9Cu_1(PO_4)_6O_{(1.5\sim2)}$	P63m	THE.	9.708	7.455
			EXP.	**9.835**	**7.405**
7	$Pb_9Cu_1(PO_4)_6O_{0.5}$	P63m	THE.	10.097	7.732
			EXP.	**9.867**	**7.460**

Acknowledgements

Thanks to Professor Kim Hyun-Tak for his guidance on this work

Supplementary materials

To ensure the authenticity and reliability of the tests, the testing was conducted by the following participants. The preparation of the samples did not involve participants in the magnetic testing. **All collaborators are responsible for their own test results.**

Table S1 Division of Experiment and Test.

Division	Sample	Contributor	Institute
Synthesis	Sample 1~7	Wang HY, Wu H, Zhou JC	CAS, IPE
Analysis		Wu ZX and Geng ZH	FZU and

PPMS	Sample 1~6	Wu H	HUST
PPMS	Figure 6	Wu H	HUST
PPMS	Sample 7	Deng ZQ	CISRI
SQUID	Sample 7	Yan LQ	CAS, IP
XRD	Sample 1~7	Wang HY	CAS, IPE
EPR	Sample 1~7	Wang HY	CAS, IPE
DFT		Chen N	USTB
XRD Ref	Sample 1~7	Chen N and Wang HY	USTB and IPE
Corresponding Author and revise		Cheng N	USTB
Original Writing		Wang HY	CAS, IPE
Funding		Ye SF and Qian P	CAS, IPE
Funding		Shi Ke	Beijing 2060

To prove the authenticity of the data, we attach two results of our testing on PPMS and other test .

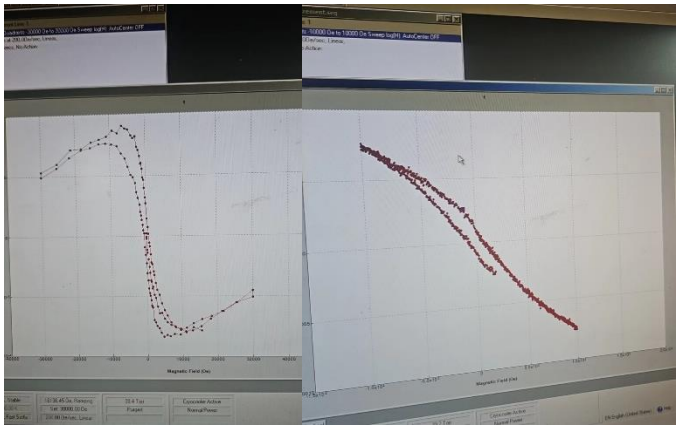

Figure S1 PPMS

Figure S2 EPR of Sample 6

The sample should be silver gray or black gray with a metallic luster. The diagram shows sample 7

Figure S3 Sample 7

Reference

[1] LEE S, KIM J-H, KWON Y-W. The First Room-Temperature Ambient-Pressure Superconductor [J]. arXiv, 2023, 2307.12008.

[2] PUPHAL P, AKBAR M Y P, HEPTING M, et al. Single crystal synthesis, structure, and magnetism of Pb10−xCux(PO4)6O [J]. APL Materials, 2023, 11(10).

[3] ZHU S, WU W, LI Z, et al. First order transition in Pb$_{10-x}$Cu$_x$(PO$_4$)$_6$O ($0.9<x<1.1$) containing Cu$_2$S [J]. arXiv, 2023, 2308.04353.

[4] THAKUR G S, SCHULZE M, RUCK M. On the synthesis methodologies to prepare Pb$_9$Cu(PO$_4$)$_6$O -- phase, composition, magnetic analysis and absence of superconductivity [J]. arXiv, 2023, 2308.05776.

[5] WU H, YANG L, XIAO B, et al. Successful growth and room temperature ambient-pressure magnetic levitation of LK-99 [J]. arXiv, 2023, 2308.01516.

[6] SINGH M, SAHA P, KUMAR K, et al. Electromagnetic properties of copper doped lead apatite Pb9Cu(PO4)6O [J]. arXiv, 2023, 2310.11051.

[7] WANG P, LIU X, GE J, et al. Ferromagnetic and insulating behavior in both half magnetic levitation and non-levitation LK-99 like samples [J]. Quantum Frontiers, 2023, 2(1): 10.

[8] LAI J, LI J, LIU P, et al. First-principles study on the electronic structure of Pb10−xCux(PO4)6O (x = 0, 1) [J]. Journal of Materials Science & Technology, 2024, 171: 66-70.

[9] YUE C, CHRISTIANSSON V, WERNER P. Correlated electronic structure of Pb$_{10-x}$Cu$_x$(PO4)$_6$O [J]. arXiv, 2023, 2308.04976.

[10] TAO K, CHEN R, YANG L, et al. The 1/4 occupied O atoms induced ultraflat band and the one dimensional channels in the Pb$_{10-x}$Cu$_{x}$(PO$_4$)$_{6}$O$_{4}$ (x=0,0.5) crystal [J]. arXiv, 2023, 2308.03218.

[11] SI L, HELD K. Electronic structure of the putative room-temperature superconductor ${\text{Pb}}_{9}\text{Cu}{({\text{PO}}_{4})}_{6}\text{O}$ [J]. Physical Review B, 2023, 108(12): L121110.

[12] LEE J B, KIM H J, LUŽNIK J, et al. Synthesis and Magnetic Properties of Hematite Particles

in a “Nanomedusa” Morphology [J]. Journal of Nanomaterials, 2014, 2014: 902968.

[13] ZHOU X, ECKBERG C, WILFONG B, et al. Superconductivity and magnetism in iron sulfides intercalated by metal hydroxides [J]. Chemical Science, 2017, 8(5): 3781-8.

[14] KIRN H T, MINAMI H, SCHMIDBAUER W, et al. Paramagnetic meissner effect in superconducting single crystals of Ba1−xKxBiO3 [J]. Journal of Low Temperature Physics, 1996, 105(3): 557-62.

[15] DASENBROCK-GAMMON N, SNIDER E, MCBRIDE R, et al. RETRACTED ARTICLE: Evidence of near-ambient superconductivity in a N-doped lutetium hydride [J]. Nature, 2023, 615(7951): 244-50.

[16] LIU Y, LIU Y-B, CHEN Q, et al. A new ferromagnetic superconductor: $$\hbox {CsEuFe}_4\hbox {As}_4$$ [J]. Science Bulletin, 2016, 61(15): 1213-20.

[17] LEE S, KIM J, IM S, et al. 상온상압 초전도체(LK-99) 개발을 위한 고찰 [J]. 한국결정성장학회지, 2023, 33(2): 61-70.

[18] KWON S-J, JUNG D-Y. A novel hybrid of high-Tc cuprate and paramagnetic organic radical [J]. Solid State Communications, 2004, 130(3): 287-91.

[19] SINGH R J, SHARMA P K, SINGH A, et al. EPR spectra of deoxygenated high Tc superconductors [J]. Physica C: Superconductivity, 2001, 356(4): 285-96.

[20] BEJJIT L, HADDAD M. EPR study, in the normal and superconducting states, of GdBa2Cu3O7 single crystal before and after grinding [J]. Physica C: Superconductivity, 2002, 371(4): 339-43.

[21] SHIMIZU H, FUJIWARA K, HATADA K. Magnetic and electronic properties of La2−xSrxCuO4 as studied by EPR of ER spin probes [J]. Physica C: Superconductivity, 1997, 288(3): 190-8.

[22] LI S-B, YIN C-H, XU Z-K, et al. Study on magnetic properties of strontium ferrite based on the technology of electron paramagnetic resonance [J]. Acta Physica Sinica, 2015, 64(10): 107502-.

[23] LIU; J, HE; C, PENG; Y-H, et al. Long-coherence pairing of low-mass conduction electrons in copper-substituted lead apatite [J]. arXiv, 2023, 2310.17160.

[24] KWON Y-W, LEE C H, CHOI D-H, et al. Materials science of DNA [J]. Journal of Materials Chemistry, 2009, 19(10): 1353-80.

[25] LEI Z, LIN C-W, CHEN I-N, et al. The characteristics of LK-99 by Cu$_2$S removal using ammonia solution: A diamagnetic semiconductor [J]. arXiv, 2023, 2309.17445.

[26] CINZIA DI G, DOMENICO D A, ANNA MARIA C, et al. Superconducting Vortex-Antivortex Pairs: Nucleation and Confinement in Magnetically Coupled Superconductor-Ferromagnet Hybrids [M]//HECTOR P-D-T. Vortex Dynamics and Optical Vortices. Rijeka; IntechOpen. 2017: Ch. 3.

[27] MOURACHKINE A. Room-Temperature Superconductivity, F, 2006 [C].